ORIENTAL JOURNAL OF CHEMISTRY
An International Open Access, Peer Reviewed Research Journal
www.orientjchem.org
ISSN: 0970-020 X
CODEN: OJCHEG
2024, Vol. 40, No.(5):
Pg. 1405-1414

Green Fabrication of SnO_2 Nanoparticles and uses as a Powerful Sorbent for Malachite Green Detoxification

ABUELIZ MODWI[1], MOHAMED ALI BEN AISSA[1], RAFIA BAKHEIT[1], ABBAS ISHAQ ALAKHRAS[2] and HAJO IDRISS[2]*

[1]Department of Chemistry, College of Science, Qassim University, Saudi Arabia.
[2]Deanship of Scientific Research, Imam Mohammad Ibn Saud Islamic University (IMSIU), Riyadh, Saudi Arabia.
*Corresponding authr E-mail: hiidriss@imamu.edu.sa

http://dx.doi.org/10.13005/ojc/400524

(Received: August 01, 2024; Accepted: September 10, 2024)

ABSTRACT

Malachite green is a poisonous and carcinogenic dye that poses serious health hazards, even at low levels, necessitating its removal from aquatic ecosystems. This study examines the use of SnO_2 nanoparticles as an adsorbent to remove MG from aquatic systems and investigates the effects of contact time, pH, and initial dye concentration on adsorption efficiency. The SnO_2 nanoparticles were synthesized employing an eco-friendly approach and characterized using various techniques, including X-ray diffraction, scanning electron microscopy, Fourier-transform infrared spectroscopy, energy-dispersive X-ray spectroscopy, and Brunauer-Emmett-Teller. The results indicate that SnO_2 nanoparticles have a high adsorption capacity for MG, reaching up to 724 mg/g with fast kinetics. The adsorption process followed the Freundlich isotherm model (R^2 = 0.987), indicating a heterogeneous adsorption mechanism. However, the kinetic data correlated well with the pseudo-second-order model (R^2 = 0.999), supporting chemisorption as the dominant process. This work shows the efficiency of SnO_2 nanoparticles as a nanosorbent for MG removal, making it a feasible option for environmental cleaning.

Keywords: SnO_2, Malachite green, Nanoparticles, Adsorption, Kinetics.

INTRODUCTION

Organic dyes, utilized in various fields, are both toxicants and carcinogens. The toxic effects of organic dyes on humans and the environment exist even at low concentrations. The persistence of organic dyes in the aquatic environment fosters severe public health and environmental problems[1]. Dyes exhibit chemical stability and structural resistance to biodegradation in both solid and aqueous environments, resulting in a prolonged life cycle upon their discharge into the environment[2]. Accumulation of dyes in aquatic environments can result in bioamplification, leading to a harmful impact on the food network[3]. Depending on the rearrangement of dyes in the environment and the formation of other dye complexes, certain initial dyes may undergo a conversion into more harmful compounds instead of retaining their original form[4]. Furthermore, it should be noted that the mere presence of fluorescent hues can have an impact on the behavioral and reproductive characteristics of fish

and certain other aquatic species[5]. Malachite green is a bright green artificial compound belonging to the triphenylmethane dye family. It finds widespread application in the textile, paper, and aquaculture sectors. Malachite Green, when introduced into the aquatic environment, exhibits high toxicity and poses substantial threats to public health. It has been determined that this substance has the potential to cause cancer in people, can cause genetic mutations in certain creatures, and can damage DNA, which may lead to the development of cancer. Even exposures that are not lethal can potentially result in the development of liver tumors, lung tumors, and cancers in the thyroid gland[6]. Therefore, it is crucial to assess the efficacy of malachite green removal in water to prevent potential environmental catastrophes and safeguard human well-being. Numerous methods have been developed for the removal of malachite green from effluents; these include adsorption, advanced oxidation processes, and membrane separation[7,8]. However, conventional methods possess some limitations, notably low efficiencies, high operational costs, or production of secondary pollutants[9]. Nanotechnology is an alternative and promising approach to treating water pollution due to its properties and higher efficiencies[10,11,12,13]. Nanomaterials, such MgO, ZnO, Al_2O_3.g-C_3N_4, carbon nanomaterials, and magnetic nanoparticles, exhibit high surface area, enhanced reaction properties, and tunable surface chemistry that can improve the ability to absorb and degrade malachite green[14,15]. They exhibit greater removal efficiencies with lower doses of material, may be applied and reused multiple times, and may be able to concentrate the dye molecules more easily than traditional materials[16]. Furthermore, nanotechnology could lead to developing novel and sustainable water treatment techniques to more effectively address dye pollution[17].

The use of plant extract methods for synthesis can be more easily scaled up when large-scale applications are required and does not pose problems associated with the need for specialized/cultivation equipment or with special cultivation conditions that are often required when working with microbial systems[18,19]. Synthesis is generally simpler and less complicated than the microbial process and does not require the complex cultivation conditions of bacteria and fungi[20]. Plant extracts are therefore more accessible to the user and less labor intensive. Some bacteria and fungi used in the synthesis of nanoparticles are pathogenic or have toxic metabolites that can cause health problems[21]. The pathogenic factors associated with handling and disposal are becoming so significant that safe disposal methods are required[22]. In addition to the pathogenic factors, the biology and by-products in the reaction mixture could also limit the purification options, resulting in a low level of purity and additional steps to purify the particles[23]. Therefore, in this work, we present a simplistic, eco-friendly, green, and cost-effective scheme for the synthesis of SnO_2 nanoparticles using plant extract of Juniperus Procera and assessed their applicability as sorbent materials for the removal of malachite green (MG) dye.

Methodology

Preparation of Juniperus Procera extract

Fresh and green Juniperus Procera leaves were harvested from trees of a plantation field located in the peri-urban zone in Al-Rass city of Saudi Arabia. The collected leaves were repeatedly rinsed with distilled water to remove impurities, dirt and substances adhering to the leaves and dried at room temperature for 7 days. The dried leaves (0.375 kg) were crushed in a mechanical blender and the resulting powder was used for the extraction process. Then the powder was mixed with 2 liters of deionized water with constant stirring (200rpm) for one day at ambient temperature and humidity. Filtration was performed afterward via Whatman No. 1 filter paper and the extract was saved in a reagent bottle at room temperature to for the purpose of serving as a reducing factor in the production of SnO_2 nanoscale.

Preparing samples for time and pH dependent Studies

For the time-dependent adsorption experiments, small portions of the SnO_2 nanoscale solution were collected at various intervals, ranging from (0 to 360 min), to observe how the adsorption efficiency changes over time. After each time point, the samples were filtered using Whatman No. 1 filter paper to separate the adsorbent from the liquid. The concentration of the target analyte in the clear filtrate was then measured. For the pH-dependent studies, the pH of the SnO_2 nanoscale solution was carefully adjusted to several values-specifically 3, 5, 7, 9, and 11

using either HCl or NaOH. Once the pH was set, the solution was stirred continuously, typically for about 60 min, to ensure ample interaction between the adsorbent and the analyte. Just like in the time-dependent studies, the samples were filtered with Whatman No. 1 filter paper, and the filtrates were analyzed to assess how the adsorption efficiency varied across different pH levels.

Fabrication and of green SnO_2 nanoparticles

To fabricate green SnO_2 nanoparticles, 90 mL of $SnCl_2$ (0.2M) was stirred slowly with 30 mL of the extract of Juniperus Procera and ultra-sonication for 15 minute. Afterward, the mixture was agitated for an extra 24 hours. Ultimately, 25 mL of KOH (3M) was added dropwise to the mixture until the precipitate formed and the obtained precipitate was isolated from the mixture using vacuum filtration. The yellowish powders were dried at 100°C for 3 h and calcined in a muffle furnace at 400°C for 1 hours.

Characterization of green SnO_2 nanoparticles

A XRD pattern was acquired to determine the crystalline nature of the manufactured SnO_2 nanopowder. A diffractometer (D8-Advance-Bruker) was operated to examine the samples with (Cu-Kα) radiation at a wavelength of 0.154nm. The morphology of the gotten nanopowder was observed under SEM. The specimens were earlier oven-dried at (105)°C and covered with (gold) to generate electrical passage on SnO_2 nanopowder. The optical properties and diffuse reflectance spectra (DRS) of the SnO_2 were determined by spectrophotometer in range 0f (300-800nm). The mode of stretching and vibration in the prepared SnO_2 was studied by FTIR (Nicolet).

Adsorption testing

To assess the adsorption situations for MG dye onto SnO_2 nanoparticles, the vestige of sorption period, sorbent mass, pH7, and initial dye quantity were examined. For the sorption investigation, 150 mL of MG dye (10 mg/L) was mixed with 60 mg of SnO_2 in a 250 mL beaker and stirred continuously at pH9. Samples were taken at different time intervals from 1 to 480 minute. Afterward, the samples were filtered, and the concentration was measured. Formula (1 and 2) were utilized for the computing elimination rate (R%) and adsorption capacity (q_t) of MG dye[24].

$$R\% = \frac{(C_o - C_t)}{C_o} * 100\% \quad (1)$$

$$q_t = \frac{(C_o - C_t)\, V}{M} \quad (2)$$

RESULT AND DISCUSSION

Characterization of SnO_2 nanoparticles

The SEM image (Fig. 1(a)) demonstrates that the nanoparticles display an irregular shape, in that they appear somewhat granular or agglomerated. From the image, it can be seen that the nanoparticles appear to be bunched together into an aggregate that does not possess a geometrically defined shape such as a sphere or a rod. Their surfaces appear rough, and some of the particles appear to have cracks or voids in between. This could be due to the sample preparation. To determine a representative particle size, several particles were manually measured from the SEM images using a ruler. The average particle size obtained from these measurements is 28.43nm. Despite variations in particle shape and size, the measurements provide a reliable estimate of the average particle size[25]. This approach ensures that the reported size reflects the overall particle distribution in the sample.

Analysis of the EDX spectrum (Fig. 1b), indicates that 2 major elements: tin (Sn) and oxygen (O), which correspond to the two main elements of tin dioxide (SnO_2). The spectrum shows, that Sn(87%) has large intensity peaks at around 3-4 keV, the Kα and Lα lines of Sn. There is also a significant peak for O(33%), about 0.5 keV. The EDX characterization confirms the successful synthesis of SnO_2 nanoparticles, in which tin and oxygen are the two predominant contributors. The spectra efficiently confirm the presence of SnO_2, giving a nod to minor discrepancies from ideal stoichiometry[26]. Fig. (1c) displays the X-ray diffraction pattern of a SnO_2 sample that was produced using Juniperus Procera extract and without it. The X-ray diffraction analysis of SnO_2 reveals distinct peaks at (110), (101), (200), (211), (220), (002), and (301) at diffraction angles of 2μ, specifically at angles of 26.5°, 33.96°, 38°, 45.2°, 54.8°, 66.1°, and 75.2°, respectively. The peaks suggest the possibility of cassiterite crystals with a tetragonal rutile structure, as documented in JCPDS No. 411445[27]. The (110) plane displays a prominent

peak of great intensity. FTIR of the SnO_2 samples, as produced, show peaks at 3409 cm^{-1} and 1630 cm^{-1}. These peaks caused from the stretching of the water surface hydroxyl group absorbed (Fig. 1d). A high spectral intensity was observed for SnO_2(extract), while SnO_2(P) showed a diminishing intensity with increasing concentration. Reduced surface area and increased crystallinity of SnO_2 contributed to the decline in spectral band intensities. In the symmetric O-Sn-O stretching mode, the oxide-bridge functional group was determined as the source of the vibration absorption band observed at around 590 cm^{-1} [28]. X-ray diffraction (XRD) analysis determined an average crystallite size of 32.05nm, calculated using the Scherrer equation., which is greater than the scanning electron microscopy (SEM) particle size of 28.42. This indicates that the crystallite size determined by XRD is measuring coherent diffraction domains while the SEM size measure is for the complete particle size. The difference is reasonable because XRD typically measures strictly crystallites within the samples particles, whereas SEM captures all dimensions of the particle shape itself, which is aligned and attests to the consistency of the structural and morphology measurements[29].

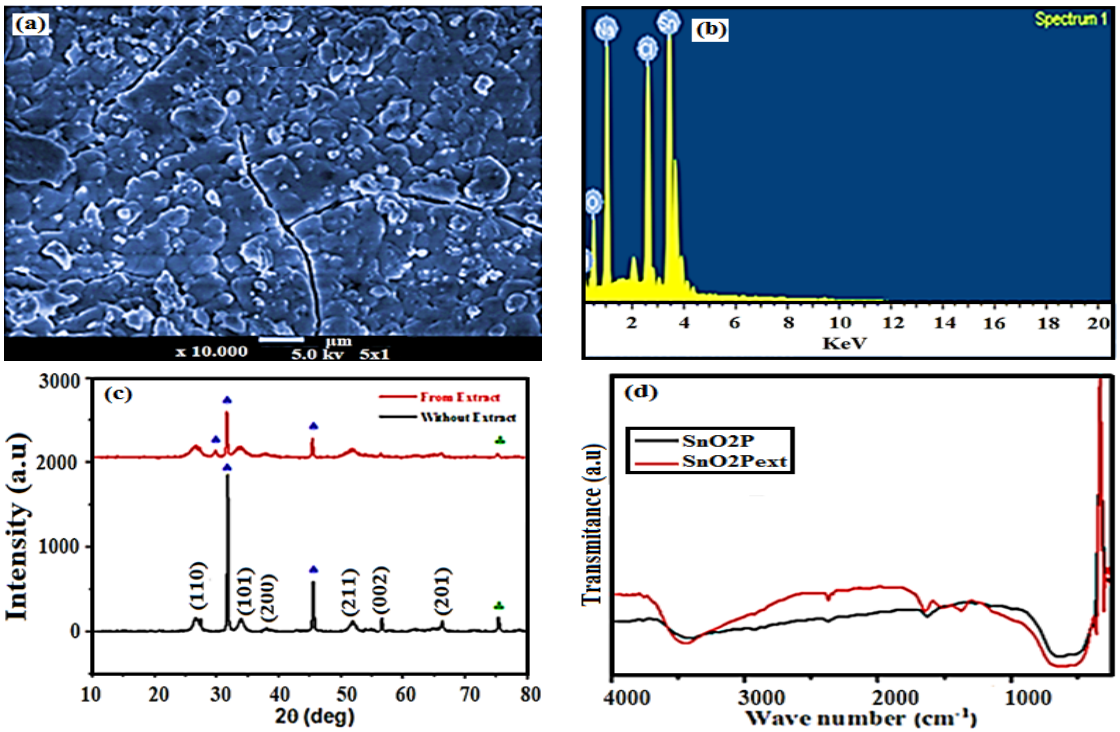

Fig. 1(a). Surface morphology of SnO_2; (b). EDX analysis of SnO_2; (c). XRD pattern of SnO_2: (d). FT-IR spectrum of SnO_2

Brunauer-Emmett-Teller (BET) analysis

The BET method was employed to estimate the specific surface area of SnO_2 by analyzing the gas adsorption and desorption isotherms. The porosity of the SnO_2 nanoparticles was also characterized through nitrogen gas adsorption and desorption processes. Fig. 2(a) and 2(b) display the adsorption and desorption isotherms, which resemble a Type IV isotherm. This isotherm is typical of mesoporous materials, known for undergoing monolayer and multilayer adsorption, leading to hysteresis and capillary condensation. Consequently, the isotherm analysis confirmed the mesoporous nature of the synthesized SnO_2 nanomaterials[30]. Further evidence of this mesoporosity was provided by the pore size distribution, also shown in Fig. 2(b). A significant proportion of the pores had a diameter of approximately 1.84nm. Although the material exhibited only a limited presence of macroscale pores, the pore distribution extended up to 250nm. The specific surface area of the material was measured to be 5.59 m^2/g. All in all, the analysis clearly points to a mesoporous structure with a diverse pore size distribution, which could have significant implications for the material's potential applications.

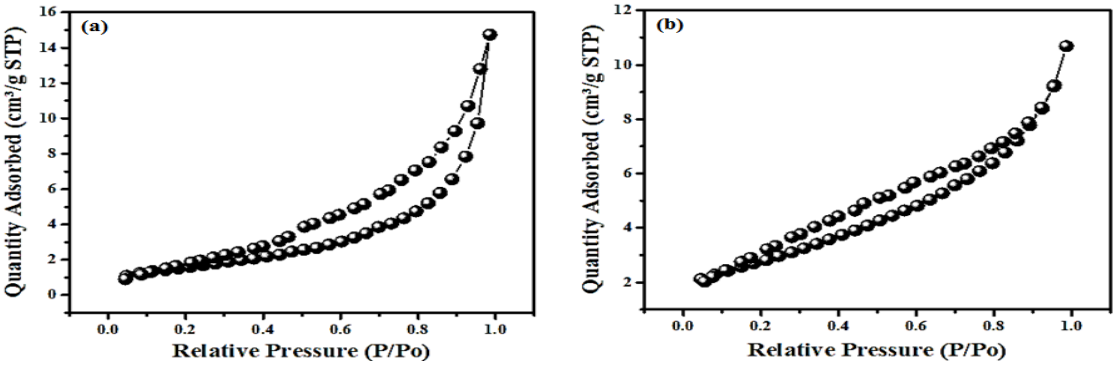

Fig. 2. Nitrogen adsorption-desorption isotherm of SnO_2 nanoparticles (a). BET surface area (b). Pore size distribution

Contact time analysis

The test was done to find out the optimal contact duration required for eliminating MG dye. Adsorption efficiency experiments were undertaken by utilizing various contact durations from (0 to 360 min), as given in(Fig. 3). The result demonstrates that the capacity of adsorption rose up from 117.4 to 468.9 mg/g as the contact duration increased from 3 min to 120 minutes. The quick rise in the absorption of pigments could be caused by surface active sites on SnO_2 nanoparticles to absorb MG[31]. Over time, the operation of adsorbing dyes slowed down and eventually reached equilibrium. This phenomenon can be explained by the saturation occurring on the surface of the SnO_2 nanosorbent and the repulsive force between the MG dye on the SnO_2 nanosorbent surface[15]. The highest removal percentage seen was 483.1% after 120 minutes.

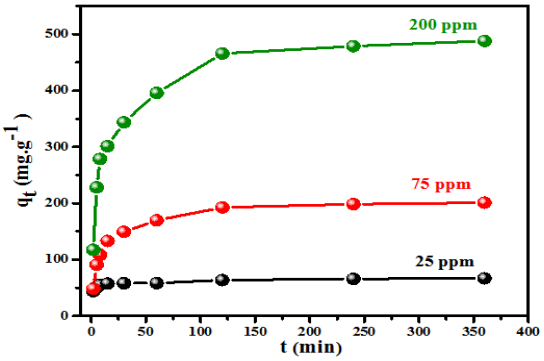

Fig. 3. Relationship between the adsorption capacity over time for various initial concentrations

pH analysis

The pH of the media strongly influences the sorption operation, as it affects both the active site and the metal's chemical state[21]. The pHpzc, or point of zero charge, is the pH value at which the surface of the adsorbent attains electrical neutrality[22]. The adsorbent surface exhibits a positive charge, as evidenced by its pHpzc value. This positive charge facilitates the adsorption of anions in solutions with pH levels below the pHpzc. Conversely, in solutions with pH values above the pHpzc, the surface acquires a negative charge, which improves cation adsorption. To determine the optimal pH for (MG) removal, pH values were systematically varied from 3 to 11. To acidify the solution, we added diluted HCl, and for basification, NaOH was used. This was done to check the concentration of each component using a pH meter. The MG removal effectiveness was assessed at each pH level under identical conditions to determine the pH at which malachite green removal considerably deviated from the surrounding levels.

From Fig. 4(a), a strong variability in the percentage removal of the contaminant with pH. A removal efficiency of about 15% is observed at pH 2, demonstrating that the adsorbent has a weak efficacy under acidic conditions. However, with increasing pH of 5, the removal percentages rise markedly to about 85%, which improves the adsorption efficacy. At a neutral pH of 7, the removal efficiency reaches a maximum close to 95%, while it peaks at about 98% at about pH 9, indicating that this is the optimum pH for adsorption. At a maximum pH of 11, the removal percentage is slightly less than before at about 90% to 95%. This could be due to changes in the surface charge of the adsorbent or possible ionization of the contaminant. This trend certainly highlights the effect of pH on the adsorption process, with maximum adsorption occurring at

neutral to slightly basic pH conditions. At elevated pH levels, the adsorption of malachite green dye by SnO_2 decreases due to the formation of hydroxyl ions and enhances the negative charge on the SnO_2 surface. This reduces the electrostatic attraction between the positively charged dye molecules and the negatively charged surface. Additionally, high pH may lead to the formation of hydroxylated or polymeric species of the dye, which are less readily adsorbed onto the SnO_2 surface. As a result, the overall adsorption capacity is diminished[32]. At low pH levels, strong interactions can occur between hydroxonium ions (H_3O^+) and the adsorbent surface. These interactions have the potential to decrease the efficiency of removing MG.

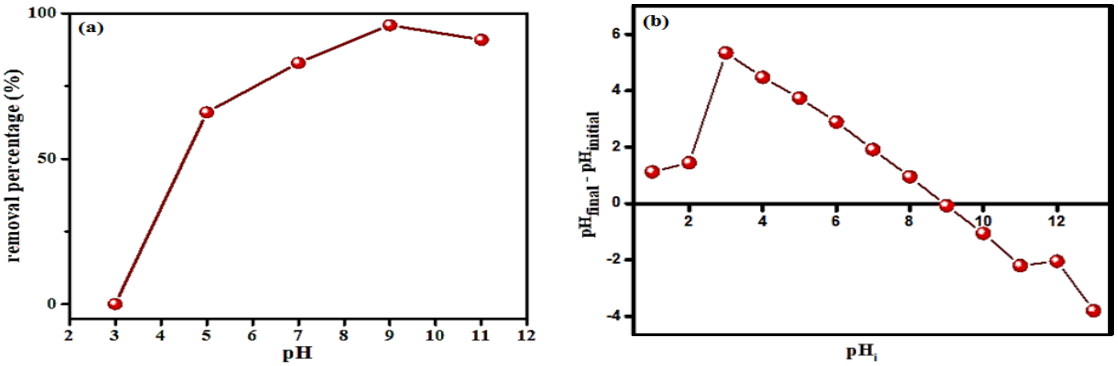

Fig. 4. Effect of pH on removal efficiency and final pH change (a). Removal percentage of MG as a function of pH (b). The difference between final and initial pH as a function of initial pH

Kinetics modeling of MG dye elimination

To assess the MG dye elimination process via SnO_2 nanoparticle, the data obtained from the adsorption experiment is examined using multiple kinetics models including the pseudo-first-order (PFO) and pseudo-second-order (PSO) models, intraparticle diffusion, and Elovich models were employed. The models are presented in the linear equation format as follows[33,34].

$$h\left(q_e - q_t\right) = h\left(q_e\right) - k_1 t \quad (4)$$

$$\frac{t}{q_t} = \frac{1}{k_2 \times q_e^2} + \frac{t}{q_e} \quad \text{PSO} \quad (5)$$

$$q_t = k_{dif}\, t^{1/2} + C \quad \text{intraparticle diffusion model} \quad (6)$$

$$q_t = \frac{1}{\beta} ln[\alpha\beta] + \frac{1}{\beta} lnt \quad \text{Elovich model} \quad (7)$$

PFO kinetics suggests that adsorption occurs by physical adsorption, whereas PSO assumes chemical adsorption (chemisorption). Chemisorption involves creating a chemical bond between an adsorbent surface and an adsorbate. Alternatively, physical adsorption is characterized by relatively gentle interactions such as hydrogen bonding, van der Waals forces, and electrostatic interactions between adsorbant and adsorbate[35]. The intraparticle diffusion model Infers that the adsorbate's internal diffusion is the slowest step, resulting in the rate controlling step during the sorption operation, and that adsorption is instantaneous. Elovich model is applied in adsorption kinetics to explains the chemical reaction process in nature[29]. Table 1 summarizes the parameters of utilized kinetic models. From the obtained results the PSO R^2 (0.999) (Fig. 7(a)) fitting is greater than PFO fitting (Fig. 5(b)) and Elovich model fitting (Fig. 5(c)) and Intra-particle Diffusion model fitting (Fig.5(d)). Therefore, the process of adsorption follows pseudo-second-order kinetics mainly because it is limited by chemisorption that occurs because stronger chemical bonds form between the adsorbate and the adsorbent. The model relies on the premise that the reaction rate is proportional to the square of the unoccupied sites, which often yields better fits for experimental data in complex surface interaction systems, or at higher concentrations of adsorbate. Furthermore, the PSO model's computed q_e is consistent with the measured qe than the PFO model. Hence, PSO is more suitable for explaining the adsorption kinetics of MG dye than PFO. This indicates that the dye sorption on SnO_2 nanosorbent is mainly mediated by chemisorption.

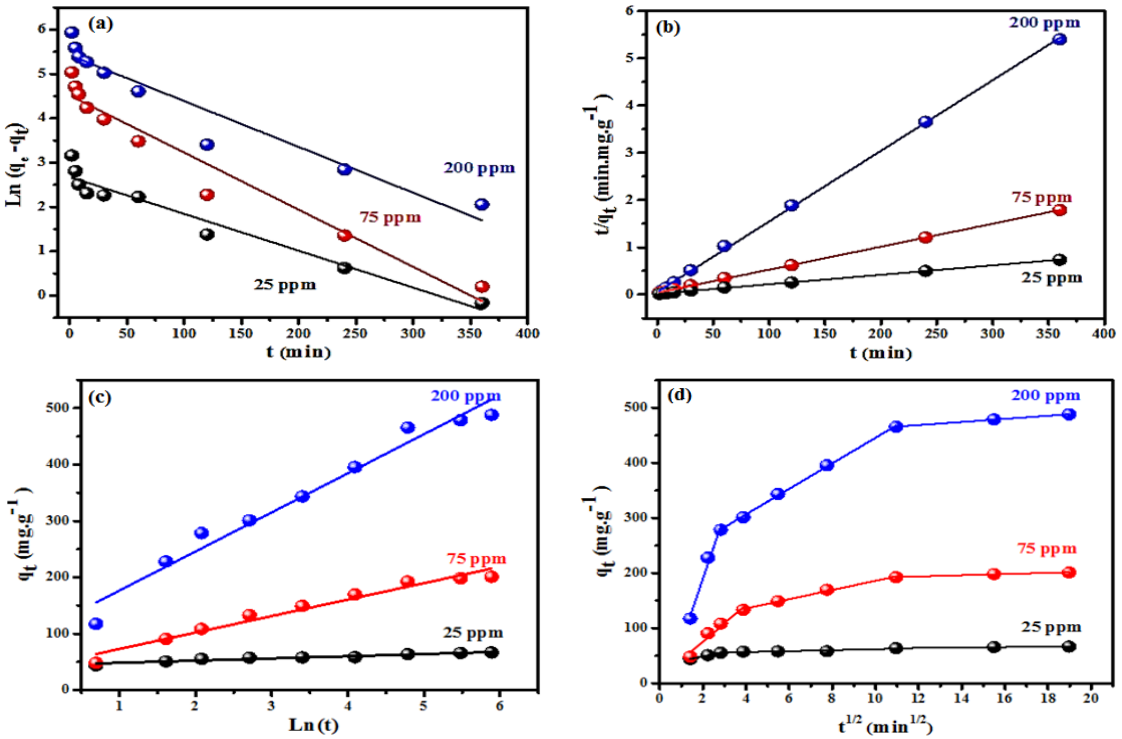

Fig. 5. Kinetics models of adsorption of MG via SnO_2 nanoparticle; (a). PFO; (b). PSO; (c). Elovich; (d). Intra-particle Diffusion

Table 1: Kinetic parameters and correlation coefficients (R^2) for different adsorption models at various initial concentrations

Kinetics Model	Parameter	25ppm	75ppm	200ppm
Pseudo-first-order	q_e	14.53	91.51	226.59
	K_1	$8.3x10^{-3}$	$12.9x10^{-3}$	$10.3x10^{-3}$
	R^2	0.947	0.952	0.925
Pseudo-second-order	q_e	66.48	205.30	500.01
	K_2	$12.05x10^{-3}$	$0.57x10^{-3}$	$0.07x10^{-3}$
	R_2	0.999	0.999	0.999
Elovich	β_2	0.256	0.034	0.014
	$_2\alpha$	1304.70	334.04	320.42
	R^2	0.929	0.966	0.969
Intra-particle Diffusion	K_{dif1}	115.22	33.79	8.08
	C1	40.94	7.61	32.54
	R2	0.985	0.956	0.998
	K_{dif2}	23.18	8.37	0.88
	C_2	213.81	102.40	53.01
	R^2	0.998	0.993	0.880
	K_{dif2}	2.79	1.07	0.39
	C_2	435.25	181.09	59.018
	R^2	0.999	0.981	0.984

Isotherm Data Analysis

Four models including {Langmuir, Freundlich, Tempkin, and Dubinin–Radushkevich (D–R)} were used to describe the experimental adsorption data[36,37].

$$\frac{C_e}{q_e} = \frac{1}{q_m} C_e + \frac{1}{q_m K_L}$$ Langmuir (linear equation) (8)

$$lnq_e = \frac{1}{n} lnC_e + h\ K_F$$ Freundlich (linear equation) (9)

$$lnq_e = lnq_m - K\varepsilon^2$$ Temkin (linear equation) (10)

$$q_e = \frac{RT}{b} lnK_T + \frac{RT}{b} lnC_e$$ Dubinin-Radushkevich (11)

In Fig. 6, the Langmuir, Freundlich, Tempkin, and Dubinin–Radushkevich isotherms are used to determine the relationship between adsorption and liquid-phase concentration. To determine the most suitable isotherm equation,

linear regression is commonly used, and correlation coefficients are used to evaluate the suitability of the equations. The examination of SnO_2 nanoparticle adsorption behaviors on MG removal revealed that the Freundlich isothermal model, with an R^2 value of 0.987, adequately explained the data. The equilibrium models parameters values of the Langmuir, Freundlich, Tempkin, and Dubinin–Radushkevich isotherm are given in Table 2. The value obtained for q_m was compared with other examined sorbent materials, as shown in Table 3. The results of the comparison shows that among the sorbents listed the SnO_2 nanoparticles are the most effective, making it a promising adrsorbent material for adsorption applications. The remarkable difference SnO_2 has in comparison to sorbents listed also highlights an advantage for utilizing advanced nanomaterials to improve adsorption efficiency. Advances like SnO_2 nanoparticles will lend themselves to a wide range of future environmental remediation applications. The comparison shows that continued research and development of nanotechnology is needed to improve adsorbents adsorption performance. The results reported here also demonstrate that nanomaterials outperform traditional adsorbents with great removal efficiencies.

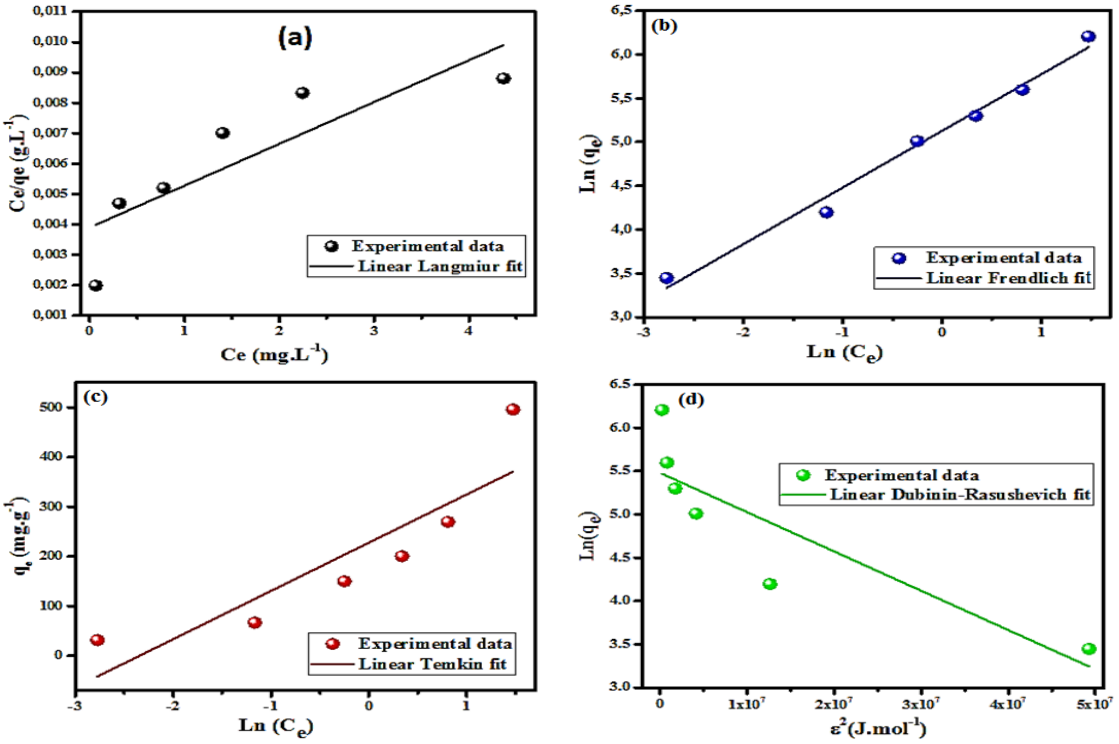

Fig. 6. Linear isotherm plots; (a). Langmuir; (b). Langmuir; (c). Temkin; (d). Dubinin-Radushkevich

Table 2: Equilibrium isotherm parameters and correlation coefficients (R^2) for various adsorption models

Equilibrium model	Parameter	Value	R^2
Langmuir	q_m	724.64	0.738
	K_L	0.35	
	R_L	0.014	
Freundlich	K_F	168.76	0.987
	n	1.54	
Temkin	B	25.48	0.779
	K_T	$4.68X10^{-4}$	
Dubinin- Radushkevich	q_m	14.90	0.757
	β	$4.54x10^{-8}$	
	E	$9.06x10^{-4}$	

Table 3: Comparison of adsorption capacities of various sorbents for malachite green dye removal

Sorbent	Adsorption capacity (mg/g)	Reference
Zeolitic imidazole frameworks	164.9	38
Carbon (nanotube)	80.60	39
Halloysite (nanotubes)	99.60	40
Activated carbon	27.80	40
Palm (fibre)	149.40	41
Rubber-wood	36.50	42
Jute fiber(carbon)	136.60	43
fly ash	170.00	44
NiO/nanoflakes	142.10	45
MgO	232.30	46
SnO_2 nanoparticles	724.00	Current study

CONCLUSION

A sustainable and cost-effective method was developed to synthesize nanoscale SnO_2. A series of batch adsorption tests of SnO_2 nanoparticles were conducted at different contact times, pH, and initial dye concentrations to assess the effectiveness of SnO_2 nanoparticles at the removal of malachite green (MG) dye. The results show that the SnO_2 nanoparticles are fast absorbers and have a high removal capacity, with a maximum experimental adsorption capacity of 724 mg/g. The kinetics of adsorption were well fitted to the pseudo-second order model (R^2 = 0.999), indicating that chemisorption was the rate-controlling phenomenon. The adsorption isotherm of MG was well described using the Freundlich model (R^2 = 0.987), suggesting that the surface sites available for adsorption on the nanoparticles are covered to some extent, thus indicating adsorption activity on a heterogeneous surface. This study confirms that the adsorption of MG on SnO nanoparticles occurs through electron transfer/sharing between a surface nanomaterial and the dye-thus further confirming the reasonableness of the adsorption capacity and mechanism.

ACKNOWLEDGEMENT

The authors extend their appreciation to the Deanship of Scientific Research, Imam Mohammad Ibn Saud Islamic University (IMSIU), Saudi Arabia, for funding this research work through Grant No. (221412017).

Conflicts of Interest

The authors declare that they have no conflicts of interest.

REFERENCES

1. Ikram, Z., *ACS Omega.*, **2024**, *9*(9), 10017-10029.
2. Ahmadi-Leilakouhi, B., *Chem. Pap.*, **2023**, *77*(2), 1033-1046.
3. Gharavi-Nakhjavani, M. S., *Environ. Sci. Pollut. Res.*, **2023**, *30*(17), 48911-48927.
4. Yan, Z., *Environ. Pollut.*, **2018**, *239*, 223-232.$_2$
5. Solayman, H. M., *J. Environ. Chem. Eng.*, **2023**, *11*(3), 109610.
6. Dowling, G., *Anal. Chim. Acta.*, **2007**, *586* (1-2), 411-419.
7. Ali, I., *J. Environ. Manage.*, **2021**, *298*, 113413.
8. Kumar, A., *Sep. Purif. Technol.*, **2022**, *287*, 120529.
9. Sharma, P., *Chemosphere.*, **2022**, *303*, 135070.
10. Chen, L., *Sep. Purif. Technol.*, **2022**, *278*, 119563.
11. Ahmed, M. J., *J. Mol. Liq.*, **2021**, *328*, 115447.
12. Zhao, S., *J. Environ. Chem. Eng.*, **2022**, *10*(5), 107218.
13. Liu, X., *Chemosphere.*, **2021**, *284*, 131356.
14. Dutta, L., *Korean J. Chem. Eng.*, **2024**, *41*(3), 589-607.
15. Saud, A., *ACS Omega.*, **2024**, *9*(27), 29088-29113.
16. Khalatbary, M., *Biomass Convers. Bioref.*, **2024**, *14*(2), 2495-2513.
17. Zhao, Y., *J. Clean. Prod.*, **2021**, *292*, 126032.
18. Alghamdi, M. D., *Inorg. Chem. Commun.*, **2024**, *159*, 111855.
19. Akhtar, M. S., *ACS Sustain. Chem. Eng.*, **2013**, *1*(6), 591-602.
20. Mittal, A. K., *Biotechnol. Adv.*, **2013**, *31*(2), 346-356.
21. Ahmed, S., *J. Radiat. Res. Appl. Sci.*, **2016**, *9*(1), 1-7.
22. Joudeh, N., & Linke, D., *Nanoscale Adv.*, **2020**, *2*(8), 3336-3347.
23. Zhang, X., *Environ. Sci. Nano.,* **2016**, *3*(6), 1274-1282.
24. Singh, P., *J. Nanopart. Res.*, **2016**, *18*(5), 166.
25. Zhang, Z., *Appl. Surf. Sci.*, **2021**, *541*, 148425.
26. Kumar, S., *Ceram. Int.*, **2022**, *48*(8), 11415-11423.
27. Rani, N., & Jaggi, N., *Bull Mater Sci.*, **2020**, *43*(1), 146.
28. Zhao, W., *Opt Mater.*, **2022**, *123*, 111934.
29. Patel, H. A., *Ceram. Int.*, **2021**, *47*(16), 22922-22930.
30. D'Arienzo, M., *Chem Mater.*, **2013**, *25*(18), 3675-3686.
31. Naggar, A. H., *Environ Sci Pollut Res.*, **2023**, *30*(49), 108247-108262.
32. Sheerazi, Z., *Biomass Conv Bioref.*, **2023**, 1-20.
33. Al-Ghouti, M. A., *J Hazard Mater.*, **2010**, *176*(1-3), 510-520.
34. Órfão, J.J.M., *J. Colloid Interface Sci.*, **2006**, *296*(2), 480-489.
35. Adeyemo, A.A., *Appl Water Sci.*, **2017**, *7*, 543-568.

36. Ismail, W.N.W., *Civil Eng J.*, **2022**, *8*(9), 1787-1798.
37. Heidarizad, M., & ₂engör, S.S., *J Mol Liq.*, **2016**, *224*, 607-617.
38. Ezzati, R., *Chem Eng J.*, **2020**, *392*, 123705.
39. Tseng.; Ru-Ling., *Chem Eng J.*, **2014**, *237*, 153-161.
40. Rodríguez-Narciso, S., *Adsorpt Sci Technol.*, **2021**, 2021, 5522581.
41. Wang, J., & Guo, X., *J Hazard Mater.*, **2020**, *390*, 122156.
42. Duran, C., *J Chem Eng Data.*, **2011**, *56*(5), 2136-2147.
43. Lin, K., *Chemosphere.*, **2015**, *139*, 624-631.₂
44. Ghaedi, M., *Phys. Chem. Chem. Phys.*, **2016**, *18*(19), 13310-13321.
45. Kiani, G., *Appl. Clay Sci.*, **2011**, *54*(1), 34-39.₂
46. Santhi, T., *Hazard. Mater.*, **2010**, *179*(1-3), 178-186.
47. Hameed, B., *J. Hazard. Mater.*, **2008**, *154* (1-3), 237-244.
48. Kumar, K., *Dyes Pigm.*, **2007**, *72*(1), 124-129.₂
49. Porkodi, K.; Kumar, K. V., *J. Hazard. Mater.* **2007**, *143*(1-2), 311-327.₂
50. Mall, I., *Colloids Surf. A: Physicochem. Eng. Asp.*, **2005**, *264*(1-3), 17-28.
51. Wei, A., *Chem. Eng. J.*, **2014**, *239*, 141-148.₂
52. Idriss, H. *J. Optoelectron. Biomed. Mater.*, **2021**, *13*(4), 183-192.